Journal of Chromatography A 1746 (2025) 465778

Contents lists available at ScienceDirect

Journal of Chromatography A

journal homepage: www.elsevier.com/locate/chroma

Direct lipid analysis of exosomes in serum by online miniaturized asymmetrical flow field-flow fractionation and electrospray ionization-mass spectrometry: Application to extrahepatic cholangiocarcinoma

Hye Ju Yu, Myeong Hee Moon *

Department of Chemistry, Yonsei University, Seoul, 03722, South Korea

ARTICLE INFO

Keywords:
Lipidomics
Exosome
Extrahepatic cholangiocarcinoma
Flow FFF
Mass spectrometry
mFlFFF-ESI-MS

ABSTRACT

Exosomes are submicron-sized extracellular vesicles involved in immune regulation, tumor metastasis, and cellular communication. Their lipid composition, distinct from parental cells, plays a crucial role in diseases like cancer. However, lipidomic analysis of exosomes, particularly in complex samples like blood, requires advanced techniques. This study optimizes miniaturized flow field-flow fractionation (mFlFFF) coupled with electrospray ionization mass spectrometry (ESI-MS) for direct lipidomic analysis of exosomes in serum. The mFlFFF technique resolves exosomes for size-based lipid analysis without prior extraction. Lipidomic profiling of serum exosomes from patients with extrahepatic cholangiocarcinoma (eCCA) identified over 1000 lipid species, with 64 showing significant changes compared to healthy controls. Target lipids were analyzed by mFlFFF-ESI-MS, revealing 35 species that distinguish eCCA patients from controls, suggesting their potential as biomarkers. Elevated levels of lysophosphatidylcholine, phosphatidylcholine, phosphatidylethanolamine, and phosphatidylinositol (PI) were observed in the eCCA group, indicating lipid alterations linked to cancer progression and inflammation. Notably, PI 38:4, involved in the release of arachidonic acid, highlights its role in inflammatory processes associated with cancer. This study demonstrates the potential of mFlFFF-ESI-MS for lipidomic analysis of exosomes and offers a non-invasive approach for cancer diagnosis, with future implications for therapeutic targeting of lipid pathways in cholangiocarcinoma.

1. Introduction

Lipids in blood are predominantly found within extracellular vesicles (EVs) and lipoproteins, the primary circulating lipid-based nanoparticles. Among EVs, exosomes are submicrometer-sized vesicles (30–150 nm in diameter) with a lipid bilayer membrane secreted by cells [1–3]. They carry proteins, DNA, RNA, metabolites, and lipids reflective of their cells of origin, enabling intercellular communication and reflecting the physiological or pathological state of the source cells [4,5]. Exosomes play significant roles in immune regulation and tumor metastasis, making them promising candidates for cancer biomarkers and therapeutic tools [6]. Notably, exosome lipid composition differs from that of parental cells, with bioactive lipids influencing recipient cell stability, inflammation, and immunity [7,8]. This has sparked interest in leveraging exosome lipids as non-invasive biomarkers and therapeutic targets [3,8–10]. Lipoproteins, another class of lipid nanoparticles, transport lipids and cholesterol between the liver and peripheral tissues via blood [11]. Classified by density, lipoproteins include high-density lipoproteins (HDL, 5–15 nm), low-density lipoproteins (LDL, 18–28 nm), and very low-density lipoproteins (VLDL, 30–80 nm) [12]. Dysregulated lipoproteins, such as reduced HDL levels or elevated, smaller LDL, are linked to cardiovascular diseases [13]. Lipidomic studies have revealed systematic lipid perturbations in lipoproteins associated with coronary artery disease, diabetes, chronic kidney disease, liver cancer, and biliary tract cancers [14–18].

Analyzing exosome lipids typically involves lipid extraction from biological fluids followed by liquid chromatography-tandem mass spectrometry (LC-ESI-MS/MS). LC-ESI-MS/MS has been widely utilized for lipid analysis and applied to cells [19], tissues [20,21], blood [22,23], urine [24], and saliva [25,26] because of the wide capability of

* Corresponding author at: Department of Chemistry, Yonsei University, 50 Yonsei-ro, Seoul, 03722, South Korea.
E-mail address: mhmoon@yonsei.ac.kr (M.H. Moon).

https://doi.org/10.1016/j.chroma.2025.465778
Received 17 December 2024; Received in revised form 12 February 2025; Accepted 13 February 2025
Available online 14 February 2025

determining lipid molecular structures with accurate quantitation. While effective, this approach risks sample loss and requires extensive preparation. An alternative is flow field-flow fractionation (FlFFF) coupled with ESI-MS/MS, which enables direct lipid analysis without lipid extraction. FlFFF separates nanoparticles like macromolecules, exosomes, and cells by size in an open channel without packing material, preserving particle integrity and avoiding clogging [27–30]. Size characterization of exosomes was achieved with FlFFF coupled to multi-angle light scattering [31–33]. Size-dependent lipidomic analysis of exosomes was carried out with urinary exosomes from patients with prostate cancer by collecting size-fractionated exosomes using FlFFF followed by nanoflow ultrahigh performance liquid chromatography-electrospray ionization-tandem mass spectrometry (nUHPLC-ESI-MS/MS) analysis of the lipid extracts of collected exosome fractions [34]. Recently, online hyphenation of FlFFF and ESI-MS/MS demonstrated its potential for lipoprotein-specific lipid analysis of human plasma samples with hepatocellular carcinoma [17]. This setup allows for direct lipid quantitation and size-based lipid distribution analysis in biological samples.

Cholangiocarcinoma (CCA), an aggressive bile duct cancer, has a five-year survival rate below 5% [35,36]. Extrahepatic cholangiocarcinoma (eCCA), a major subtype, lacks reliable diagnostic and prognostic biomarkers [37–39]. Efforts have identified circulating nucleic acids and glycoproteins such as CA19-9 [40] and CA125 [41], respectively, but these have limited sensitivity and specificity. Lipid biomarkers for eCCA remain underexplored, though studies have noted phosphatidylcholine (PC) 34:1 overexpression in tumor samples with iCCA [42] and alterations in the serum levels of lysophosphatidylcholine and lysophosphatidylethanolamine species between iCCA and HCC [43]. However, lipid analysis regarding to eCCA has rarely been made and lipids contained in exosomes from serum or plasma samples with eCCA have not been investigated yet. Most analyses require extensive preparation, such as lipid extraction or proteolysis, prior to LC-ESI-MS/MS.

This study introduces a miniaturized FlFFF (mFlFFF) directly coupled with ESI-MS for size separation and lipid quantitation of exosomes isolated from serum samples. The direct hyphenation of FlFFF with MS via ESI enables size-based fractionation of exosomes by FlFFF, followed by real-time MS analysis of exosomal lipids without the need for preliminary lipid extraction. Conventional lipid extraction, which typically requires several hours and organic solvents before LC-ESI-MS/MS analysis, is bypassed in this approach. The key advantage of mFlFFF-ESI-MS/MS is its ability to streamline this process, enabling high-speed lipid quantification of exosomes from serum samples without lipid extraction.

This study first assessed lipid perturbations between the eCCA and healthy control groups using nUHPLC-ESI-MS/MS to identify target lipids. Next, mFlFFF was optimized to operate at microflow rate scales compatible with ESI-MS, allowing for the direct lipidomic profiling of serum exosomes from eCCA patients based on the selected target lipids. This approach facilitated the screening and identification of key lipids for subsequent mFlFFF-ESI-MS analysis. Statistical evaluations revealed candidate lipid biomarkers, demonstrating the utility of mFlFFF-ESI-MS as a powerful tool for non-invasive lipid analysis and its potential for advancing eCCA diagnostics.

2. Experimental

2.1. Materials and reagents

A total of 42 lipid standards with odd-numbered and deuterated acyl chains were purchased from Avanti Polar Lipids, Inc. (Alabaster, AL, USA), as listed in the Supplementary Materials (T1). Reagents included ammonium bicarbonate (NH_4HCO_3), ammonium hydroxide (NH_4OH), ammonium formate (NH_4HCO_2), sodium azide (NaN_3), SDS, sodium chloride (NaCl), sodium phosphate dibasic heptahydrate ($Na_2HPO_4{\cdot}7H_2O$), potassium chloride (KCl), potassium phosphate monobasic (KH_2PO_4), and carbonic anhydrase, all obtained from Sigma-Aldrich (St. Louis, MO, USA). High-performance liquid chromatography (HPLC)-grade solvents (acetonitrile, chloroform, isopropyl alcohol, methanol, methyl tert-butyl ether, and water) were from Avantor Performance Materials (Center Valley, PA, USA). Fused silica capillary tubes (i.d. 50–200 μm, o.d. 360 μm) were from Polymicro Technologies, LLC (Phoenix, AZ, USA). Pierce Albumin/IgG Removal Kits and Nanosphere™ size standards were purchased from Thermo Fisher Scientific (Waltham, MA, USA). The detailed information regarding the instruments and equipment used in this study are provided in the Supplementary Materials (T2).

2.2. Human serum samples

Serum samples from healthy controls ($n = 10$, age 61.7 ± 4.5 years) and eCCA patients ($n = 10$, age 69.3 ± 8.2 years) were obtained from the Chungbuk National University Hospital Biobank, Korea, with informed consent under IRB-approved protocols. Samples were stored at −80 °C. High-abundance proteins were removed using the Pierce Albumin/IgG Removal Kit prior to mFlFFF analysis.

2.3. Isolation of exosomes

Serum samples (500 μL) were thawed at 4 °C and centrifuged sequentially at 1,000 × g for 15 min to remove cell debris and at 12,000 × g for 30 min to eliminate microvesicles. The supernatant was processed to isolate exosomes using ultrafiltration (UF) with Vivaspin® centrifugal concentrators (MWCO 300 kDa) from Sartorius AG, Goettingen, Germany, at 5,000 × g for 30 min at 4 °C. The initial sample volume for exosome isolation using the UF method was optimized by varying the serum volume. The efficiency of the UF method in exosome isolation was compared with the conventional ultracentrifugation (UC) method, as described in the Supplementary Materials (T4), by assessing the number of lipids identified and quantified from the isolated exosomes. The retentate was collected in 0.01 M PBS (100 μL) and stored at 4 °C. The sample preparation approaches were selected according to the specific goals of each technique. In nUHPLC-ESI-MS/MS, two pooled samples from the eCCA patients and healthy controls were used to select target lipids. In contrast, individual samples were used in mFlFFF-ESI-MS to analyze the selected target lipids, incorporating individual variability.

2.4. Lipid extraction for nUHPLC-ESI-MS/MS analysis

Exosome samples were lyophilized and extracted using CH_3OH (300 μL) in an ice bath, followed by the addition of MTBE (1 mL) and vortexing for 1 hour. After phase separation with MS-grade water (250 μL) and centrifugation (1,000 × g, 10 min), the organic layer was transferred, and the aqueous phase was re-extracted with MTBE (300 μL) and centrifuged (1,000 × g, 10 min). The pooled organic extracts were dried under N_2 gas, weighed, and dissolved in CH_3OH:$CHCl_3$:H_2O (18:1:1, v/v) at 5 μg/μL. Internal standards (Supplementary Table S1) were added before storage at −80 °C.

2.5. nUHPLC-ESI-MS/MS

Lipid analysis using nUHPLC-MS/MS was carried out with non-targeted identification of the lipid species in exosomes isolated from pooled serum samples (the control and the eCCA group each) in data-dependent MS/MS scan mode, followed by a targeted quantitation of the identified lipids in the full MS scan using the polarity switching mode. Lipidomic analysis was performed using a Dionex Ultimate 3000 RSLCnano System coupled with a Q-Exactive Orbitrap MS (Thermo Fisher Scientific, San Jose, CA, USA). The analytical column was prepared in our laboratory using a silica capillary tube (100 μm of i.d. and

360 μm of o.d.) of which one end was pulled by flame to create a sharp tip. Then the tip portion (~ 1 cm) of a column was packed with Watchers® ODS-P C-18 particles (3 μm and 100 Å) purchased from Isu Industry Corp. (Seoul, Korea) to create a self-assembled frit. Then, BEH Shield C18 particles (1.7 μm and 130 Å) unpacked from ACQUITY UPLC BEH Shield RP18 column (2.1 mm x 100 mm) purchased from Waters (Milford, MA, USA) were used to pack the remaining column space (7.0 cm). The column was connected to the nUHPLC pump via a nanoViper tube (20 μm i.d.) and a stainless steel MicroTee from IDEX Health & Science (Oak Harbor, WA, USA), with the other port of the MicroTee connected to a Pt wire for delivering a high voltage (~ 3 kV) for ESI. A binary gradient elution was performed using mobile phases A (H_2O/ACN 9:1, v/v) and B (IPA/CH_3OH/ACN/H_2O 7:1.5:1:0.5, v/v/v/v), both containing ionization modifiers (5 mM NH_4OH and 0.5 mM NH_4HCO_2) to perform ESI in both positive and negative ion modes for MS. Sample loading was performed with 100% mobile phase A at a flow rate of 800 nL/min. The gradient elution progressed as follows: mobile phase B was increased to 75% over 5 min, to 80% over the next 5 min, to 100% over the subsequent 5 min, and maintained at 100% for 10 min. The column was reconditioned with 100% phase A for 5 min, followed by a reduction of flow rate to 0 nL/min and a 2-minute hold to relieve pressure to 0 bar before the next run.

Lipid structures were determined using the LipidMatch software [44] by analyzing MS/MS spectra, with manual verification. Lipid identification was based on the exact mass of the precursor ion, with a tolerance of 5 ppm, retention time, and the characteristic MS/MS spectra for each lipid. For quantification, lipid classes including lysophosphatidylcholine (LPC), phosphatidylcholine (PC), EtherPC, lysophosphatidylethanolamine (LPE), phosphatidylethanolamine (PE), EtherPE, sphingomyelin (SM), ceramide (Cer), hexosylceramide (HexCer), diacylglycerol (DG), triacylglycerol (TG), and cholesteryl ester (CE) were detected in the positive ion mode, while lysophosphatidic acid (LPA), phosphatidic acid (PA), lysophosphatidylserine (LPS), phosphatidylserine (PS), lysophosphatidylglycerol (LPG), phosphatidylglycerol (PG), lysophosphatidylinositol (LPI), phosphatidylinositol (PI), and cardiolipin (CL) were quantified in the negative ion mode during polarity switching. MS instrument parameters for nUHPLC-ESI-MS/MS analysis are outlined in Table S2a. Lipid quantification was achieved with calibration curves of each lipid class that were constructed using the normalized peak area, which is the ratio of a specific lipid's peak area to that of the corresponding internal standard (IS), in five replicate runs of nUHPLC-ESI-MS/MS. Peak areas were calculated using Xcalibur software from Thermo Scientific.

2.6. mFlFFF-MALS-UV and mFlFFF-ESI-MS

The mFlFFF channel used in this study was modified from a model LC channel by Wyatt Technology Europe GmbH (Dernbach, Germany) through the replacement of the original inlay with a custom-built polycarbonate inlay. The inlet hole was positioned 7.2 cm from the outlet hole, as shown in Figure S1. The metal clamping block was also substituted with a custom block designed to accommodate the reduced channel dimensions. The trapezoidal channel had triangular breadths of 0.80 cm and 0.15 cm at the inlet and outlet, respectively. Three different Mylar sheet thicknesses (100,170, and 190 μm) were employed to optimize the separation of exosomes within the reduced channel dimensions. Carrier solutions were prepared using ultrapure water (>18 MΩ·cm) with 0.05% SDS and 0.02% NaN_3 for PS separation, and 10 mM NH_4HCO_3 for exosome separation during mFlFFF-ESI-MS. Both solutions were filtered through a mixed cellulose ester (MCE) membrane filter (pore size 0.22 μm, MF-Millipore®; Danvers, MA, USA). Sample injection was carried out with a 7725i loop injector (Rheodyne®; Cotati, CA, USA), in combination with a carrier solution delivered by a SP930D HPLC pump (Young-Lin Instrument Co.; Seoul, Korea). Focusing and relaxation of the sample were performed approximately 1/10th of the way down the channel. The channel membrane was composed of regenerated cellulose with a molecular weight cut-off of 10 kDa.

For the optimization of exosome separation, serial detection was conducted using a DAWN HELEOS II multi-angle light scattering (MALS) detector (Wyatt Technology; Santa Barbara, CA, USA) and a UV730D UV/Vis detector (Young-Lin Instrument Co.; Anyang, Korea), as shown in Fig. 1. Exosome size was calculated using ASTRA software (Wyatt Technology) based on the Zimm method. During the FlFFF separation, size fractions were collected for Western blot analysis to verify the presence of exosomes and lipoproteins, with details available in the Supplementary Materials, T3.

For mFlFFF-ESI-MS analysis of serum exosomes, the effluent from the mFlFFF was merged with an ionization modifier solution (5 mM NH_4OH and 1.0 % HCO_2H in a 5:5 v/v ACN/MeOH mixture) from a syringe pump at a flow rate of 70 μL/min, using a microTee. The combined flow was directed to the Q-Exactive Orbitrap MS system via the HESI-II probe (Fig. 1). MS instrument parameters for mFlFFF-ESI-MS are detailed in Table S2b. Lipid quantification was performed by full MS scan of the exact mass of the precursor ions, with a tolerance of 5 ppm. Student's *t*-test was conducted using SPSS software (version 26, IBM Corp., Armonk, NY, USA), and principal component analysis (PCA) was performed using Minitab 17 (Minitab, Inc., State College, PA, USA).

3. Results & discussion

3.1. Optimization of exosome separation by mFlFFF-MALS-UV

The performance of the mFlFFF channel in separating nanometer-sized particles was evaluated using channels of three different thicknesses: 100, 170, and 190 μm. A critical aspect for successfully size-separating exosomes and enabling simultaneous exosomal lipid analysis by ESI-MS was optimizing the outflow rate, $\dot{V}_{out}$. Polystyrene standard latex particles (20,50, 100, and 200 nm in diameter) were used to test flow rate conditions, especially for direct hyphenation with ESI-MS. When a 100 μm-thick channel was used (Figure S2a), $\dot{V}_{out}$ could be reduced to 50 μL/min under a crossflow rate, $\dot{V}_c$, of 250 μL/min, enabling resolution of particles up to 100 nm. However, 200 nm particles were not recovered due to the high field strength. Increasing the channel thickness from 100 μm to 170 μm (Figure S2b) along with an increase in $\dot{V}_{out}$ to 70 μL/min and a decrease in $\dot{V}_c$ to 30 μL/min, successfully facilitated the elution of 200 nm particles; however, significant tailing was observed. By further reducing $\dot{V}_c$ to 20 μL/min, reasonable separation with enhanced elution of 200 nm particles was achieved (Fig. 2, bottom) Under the optimized conditions, serum-derived exosomes from a healthy individual were analyzed using mFlFFF-MALS-UV (Fig. 2, top). The root-mean-square (RMS) radius (R_g) values of exosomes, calculated during the elution time course, were superimposed with light scattering signals at 90°, indicating size-based fractionation was achieved. The size range of exosomes was measured to be ~34.0–68.5 nm in radius (~68.0–137.0 nm in diameter). Since the hydrodynamic radius (R_h) is expected to be similar to R_g for hollow spheres with negligible shell thickness, the exosomal R_h is likely comparable to or slightly larger than R_g, reflecting the thin but finite thickness of the exosome structure.

3.2. Selection of target lipids from serum exosomes with extrahepatic cholangiocarcinoma

Before direct lipid analysis of serum-derived exosomes using mFlFFF-ESI-MS, a quantitative lipidomic analysis was performed to identify lipid species significantly altered in exosomes from extrahepatic cholangiocarcinoma (eCCA) patients compared to healthy controls using nanoflow UHPLC-ESI-MS/MS. For this analysis, lipid extracts from exosomes isolated using UF from 0.5 mL serum samples were analyzed. The serum volume was optimized to 0.5 mL based on the number of identified lipids and relative lipid levels as explained in Supplementary

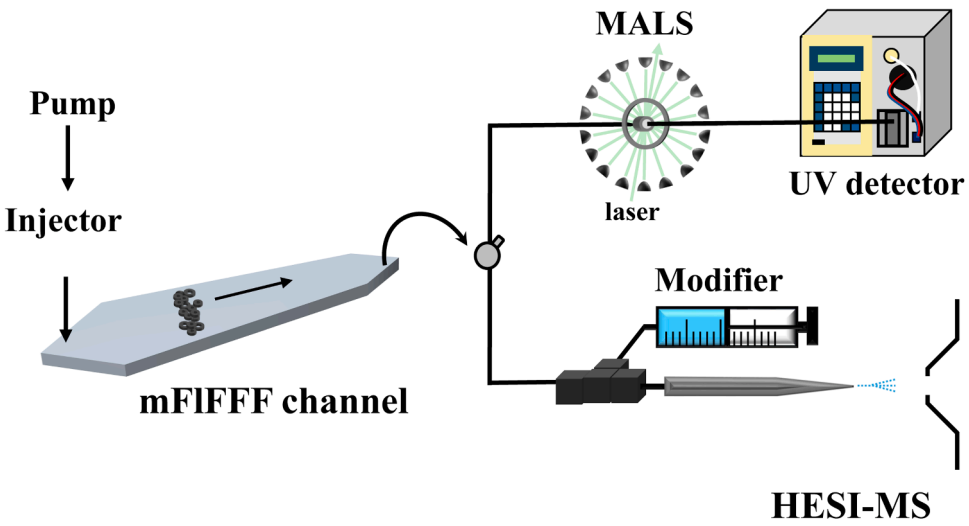

Fig. 1. Schematic illustrating the miniaturized mFlFFF system coupled with MALS-UV for size characterization and ESI-MS for lipid analysis.

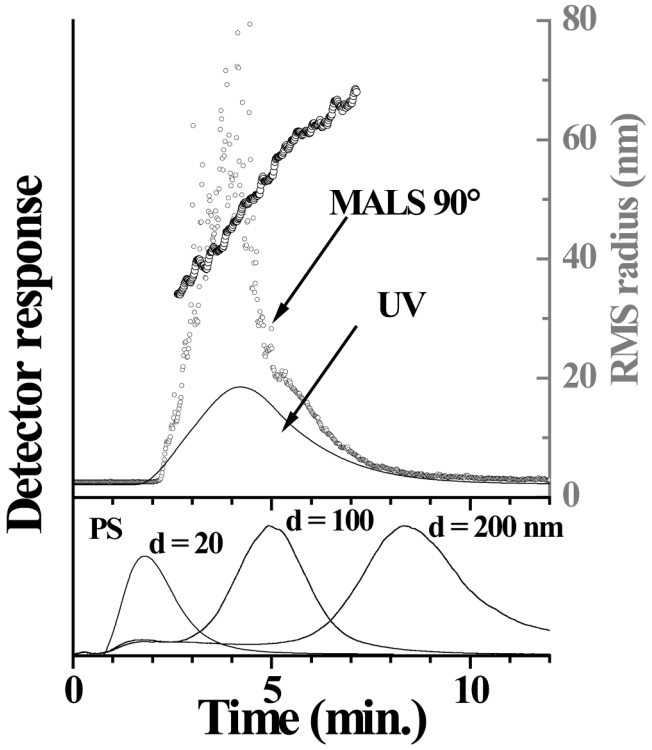

Fig. 2. Separation of serum exosomes and polystyrene beads using mFlFFF-MALS-UV. (Top) Exosome size distribution with RMS radius (R_g) profiles. (Bottom) Separation of polystyrene beads demonstrating resolution of particles up to 200 nm in diameter (d).

Materials (Figure S3).

Lipidomic profiling was performed on pooled serum exosome samples from eCCA patients (n = 10) and controls (n = 10). Due to the limited serum volume (~0.6 mL per individual), a pooling strategy was applied for each group to identify the significantly altered lipid species in eCCA, which were then saved for mFlFFF-ESI-MS analysis at the individual level. A previous study on lipoprotein lipids, using both analytical methods, demonstrated the similarity in quantification of target lipids [17]. Therefore, this study focused on utilizing pooled serum samples for the selection of target lipids. A total of 1119 lipid species were identified in the eCCA group, compared to 1051 in controls. Among these, 246 lipid species in eCCA and 217 in controls were quantified using calibration curves for each lipid class. Limit of detection (LOD, S/N = 3) ranged from 0.012 to 0.174 nmol/mL, while limit of quantification (LOQ, S/N = 10) ranged from 0.039 to 0.581 nmol/mL (Table S3). Detailed individual lipid concentrations for both groups are presented in Table S4 and the isomeric structures of each molecular species confirmed from MS/MS experiments are listed in Table S5. Lipid quantification revealed total levels of most lipid classes (e.g., PC, PE, PA, PS, and DG) were higher in eCCA than controls, except for EtherPE, PS, and TG (Figure S4). From these results, 64 lipid species with significant alterations (>1.5-fold change between eCCA and controls) were selected as target lipids for further analysis (Figure S5, Table S6). These include both upregulated and downregulated species, with fold ratios and concentrations detailed in supplementary materials. These findings provide a robust basis for comparative analysis of exosomal lipids using mFlFFF-ESI-MS.

3.3. Top-down lipid analysis of serum exosomes by mFlFFF-ESI-MS

Direct lipid analysis of exosomes was performed by injecting isolated serum exosomes into the mFlFFF-ESI-MS system. This approach enabled size-based fractionation and real-time analysis of lipid profiles within the exosomes. Using the 64 lipid species identified as significantly altered in the bottom-up analysis with nUHPLC-ESI-MS/MS, top-down lipid quantification was conducted for individual samples (10 eCCA patients and 10 healthy controls).

Fig. 3a displays the extracted ion fractograms (EIFs) of PC 34:1 (m/z 760.585) from mFlFFF-ESI-MS runs for each exosome sample (10 patients and 10 controls). These results highlight variations in PC 34:1 levels between the groups, with the eCCA group showing a significant increase (1.71 ± 0.31-fold, p = 0.0007). Since the current study focused on demonstrating the capability of mFlFFF-ESI-MS for high-speed screening of target lipids, MS analysis with mFlFFF was carried out in precursor scan mode without differentiating the regioisomeric structures of phospholipids. Similarly, differences in the profiles of other lipid classes are illustrated in Fig. 3b. Notably, peak distributions of PE 38:4 and PI 38:4 appear narrower compared to those of SM d42:2, suggesting that lipid distributions vary with exosome size and lipid composition in serum. Reproducibility of the mFlFFF-ESI-MS analysis was estimated by calculating the percent relative standard deviation (%RSD) of the concentrations of the five lipid species shown in Fig. 3 across three replicate measurements. The average %RSD for these measurements was 3.2%, as shown in Table 2. The same calculation for data obtained by nUHPLC-ESI-MS/MS resulted in a 3.5% %RSD based on five replicate

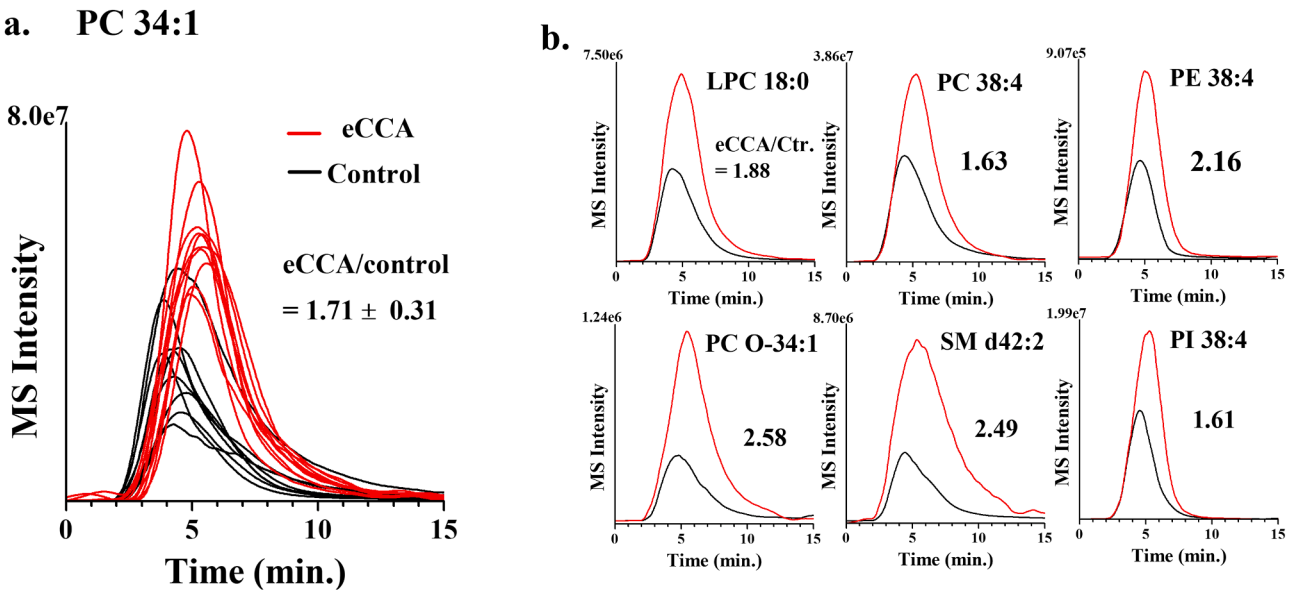

Fig. 3. Direct lipid profiling of serum exosomes using mFlFFF-ESI-MS. Extracted ion fractograms (EIFs) for selected lipid species are shown, highlighting the elution profiles of high-abundance lipids in the eCCA ($n = 10$) and control ($n = 10$) groups. Differences in signal intensity indicate upregulation of lipid species such as PC 34:1 in eCCA.

measurements.

To confirm the elution of exosomes, four fractions were collected from the mFlFFF outlet and analyzed using Western Blot for proteins specific to HDL (ApoA1), LDL/VLDL (ApoB), and exosome markers (CD63 and CD81). All fractions showed responses for CD63 and CD81, confirming the presence of exosomes in Fig. 4. ApoA1 was detected in fraction F1; however, the MS intensity of lipids in this fraction, likely from residual HDL particles and exosomes, was relatively low. This supports the effective removal of most HDL particles during exosome preparation by the ultrafiltration method. However, ApoB signals in some fractions indicated incomplete removal of VLDL, which overlaps in size with exosomes (30–80 nm for VLDL vs. 30–150 nm for exosomes). This highlights the challenge of fully separating exosomes from serum lipoproteins.

Fig. 5a presents a statistical comparison of the quantified lipids between the eCCA and control groups using Principal Component Analysis (PCA). This analysis clearly distinguishes the two groups based on individual lipid profiles with the first principal component showing a variance of 20.2%, despite some variation within each group. Fig. 5b shows a volcano plot, where the statistical p-values of the 64 target lipids are plotted against the $\log_2$ (fold ratio = eCCA/control). The majority of target lipids exhibited significantly higher levels in the eCCA group ($p < 0.05$ and fold change > 1.5, located in the upper right domain of the plot). Only those lipids showing significant differences ($p < 0.05$ and > 1.5-fold change) are visualized in Fig. 5c as a heatmap, illustrating the distinct increases in the eCCA group.

The quantified lipid results from mFlFFF-ESI-MS were further compared to nUHPLC-ESI-MS/MS results. Table 1 compares the

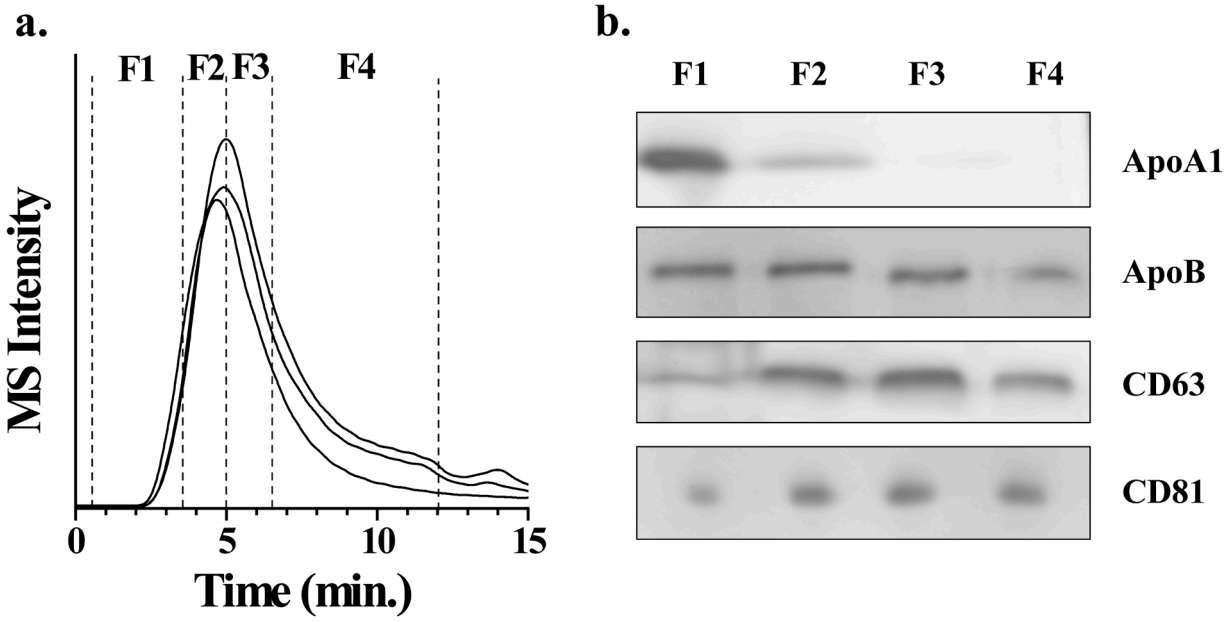

Fig. 4. mFlFFF fractograms of a) serum-derived exosome isolates from healthy controls (three repeated runs) and b) Western blot results using specific markers, ApoA1 (for HDL), ApoB (for LDL/VLDL), and CD63 and CD81 (for exosomes).

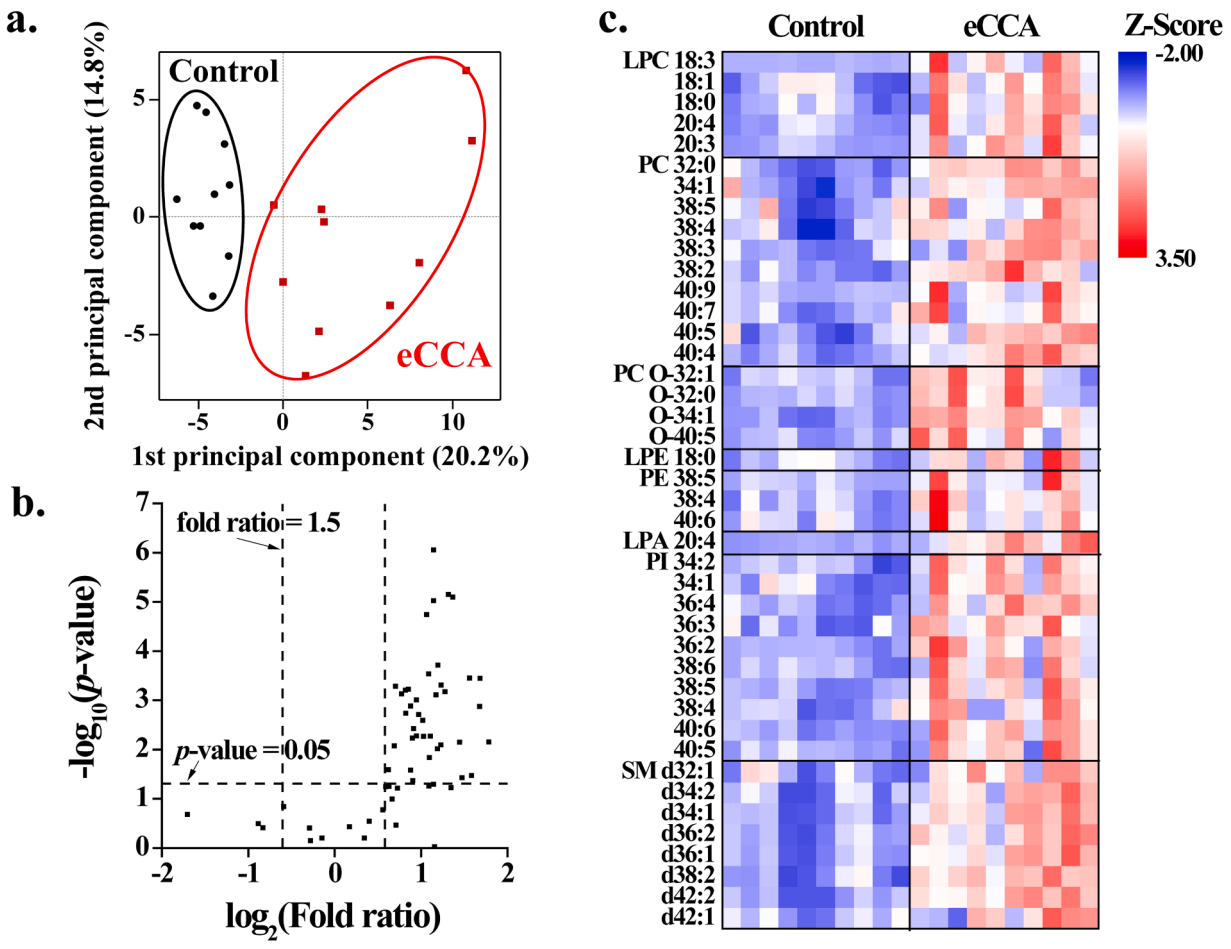

Fig. 5. Statistical comparison of lipid profiles between eCCA and control groups. (a) PCA shows clear separation of the two groups, based on individual lipid profiles. (b) Volcano plot illustrates lipid species with significant fold changes (>1.5-fold, $p < 0.05$), with most lipids increased in the eCCA group (upper right). (c) Heatmap of significantly altered lipids, highlighting elevated lipid levels in eCCA samples. Color intensities represent fold changes relative to controls.

calculated fold ratios (eCCA/control) for the 35 lipid species that showed significant differences (>1.5-fold, $p < 0.05$, and AUC > 0.800) in the eCCA group by mFlFFF-ESI-MS, based on 64 targets. Since the nUHPLC-ESI-MS/MS quantification was based on pooled samples, the standard deviation representing the individual variation and statistical *p*-values comparing the two groups were not available. However, *p*-values in Table 1 were obtained from Student's *t*-test between mFlFFF-ESI-MS results of the eCCA and healthy normal individuals. The relative errors in the fold ratios of most lipids obtained by mFlFFF-ESI-MS were not significantly high, except for few species, including LPC 18:3 (28.7%) and LPC 20:3 (32.9%). The relatively higher standard deviation in fold ratios was attributed to fluctuations in MS intensity for low-abundance species. The %RSD values for individual measurements of LPC 18:3 averaged 11.5% for the control group and 12.1% for the eCCA group, whereas a high-abundance species such as LPC 18:0 exhibited lower %RSD values of 6.0% (control) and 4.8% (eCCA). Among the 35 lipid species listed in Table 1, seven low-abundance species (LPC 18:3, LPC 20:3, PC 38:2, PC 40:4, PC 40:9, Ether PC O32:0, and LPA 20:4) displayed relatively higher errors in fold ratio measurements using mFlFFF-ESI-MS. These elevated errors in the analysis of low-abundance lipid species likely result from ion suppression caused by high-abundance species when exosome lipids are simultaneously introduced into the ESI-MS. In contrast, liquid chromatography enables a more detailed separation of lipid species, reducing spectral congestion in nUHPLC-ESI-MS/MS analysis.

Further statistical analysis through receiver operating characteristic (ROC) curve analysis was applied to identify candidate lipid species that could distinguish eCCA from control serum exosome lipids based on mFlFFF-ESI-MS results. ROC analysis identified 35 lipid species meeting the criteria (AUC > 0.800 as well as > 1.5-fold change and $p < 0.05$), where AUC represents the area under the curve. Fig. 6 presents ROC curves for six high-abundance species, while Figure S6 includes the remaining candidates. Table 1 lists the AUC values and fold ratios (eCCA/control) for these 35 lipid species, with statistical significance determined by *t*-tests comparing mFlFFF-ESI-MS results to the nUHPLC-ESI-MS/MS reference values which were based on repeated measurements from pooled samples. The results demonstrate that mFlFFF-ESI-MS enables robust, high-throughput top-down lipidomic analysis of serum exosomes, revealing significant alterations in lipid profiles associated with eCCA. These findings contribute to the growing body of evidence supporting the role of lipidomics in understanding exosome biology and its relevance to cancer pathophysiology.

Given the limited studies on lipid analysis in cholangiocarcinoma, correlating the lipid alterations observed in this study with disease pathophysiology remains challenging. However, some reports have provided valuable comparisons. For instance, a study on hepatocellular carcinoma (HCC) patients compared to those with intrahepatic cholangiocarcinoma (iCCA) reported significant alterations in serum levels of LPC species, with LPC 18:0 and 20:3 upregulated, and LPC 18:3 and 20:4 downregulated in HCC patients [45]. In contrast, our study found a simultaneous increase in these LPC species in the eCCA group. A recent lipidomic analysis of bile-derived exosomes from malignant cholangiocarcinoma (CCA) patients revealed similar findings, with most lipid species, particularly PC, significantly increased in malignant cases

Table 1
Comparison of calculated fold ratios (eCCA/Control) for 35 selected lipids in serum exosomes showing significant differences (>1.5-fold, $p < 0.05$, and AUC > 0.800) by mFlFFF-ESI-MS based on 64 targets established by nUHLC-ESI-MS/MS. The *p*-values of the *t*-test were calculated by comparing the mFlFFF-ESI-MS measurements with nUHPLC-ESI-MS/MS data as a reference value at a 95 % confidence level.

		nUHPLC-ESI-MS/MS	mFlFFF-ESI-MS		
class	acyl chain	Fold ratio (eCCA/control)	Fold ratio (eCCA/control)	AUC value	*p*-value
LPC	18:0	2.23	1.88 ± 0.28**	0.854	0.16
	18:3	2.01	8.85 ± 2.54**	0.979	0.017
	20:3	2.07	6.61 ± 2.18**	0.938	0.011
	20:4	2.12	4.68 ± 1.60**	0.875	0.024
PC	32:0	1.83	2.21 ± 0.35**	0.979	0.011
	34:1	1.6	1.71 ± 0.31**	0.917	0.319
	38:2	1.54	2.96 ± 0.76**	0.979	0.003
	38:3	1.96	2.03 ± 0.40**	0.833	0.786
	38:4	1.72	1.63 ± 0.19**	0.917	0.416
	38:5	1.69	1.54 ± 0.27*	0.896	0.376
	40:4	1.95	3.22 ± 0.57**	1.000	0.014
	40:5	1.83	2.43 ± 0.68**	0.917	0.029
	40:7	1.58	2.28 ± 0.51**	0.917	0.102
	40:9	1.52	5.58 ± 2.14*	0.854	0.04
Ether PC	O-32:0	2.16	3.45 ± 0.81**	0.875	0.101
	O-32:1	1.54	2.14 ± 0.43*	0.875	0.144
	O-34:1	2.28	2.58 ± 0.39**	1.000	0.156
	O-40:5	2.15	1.93 ± 0.27**	0.979	0.412
PE	38:4	1.59	2.16 ± 0.49**	0.896	0.11
	38:5	1.56	3.00 ± 0.85*	0.896	0.104
LPA	20:4	2.08	3.20 ± 0.60**	0.979	0.045
PI	34:1	1.72	1.84 ± 0.28**	0.854	0.527
	34:2	2.02	1.96 ± 0.28**	0.875	0.805
	36:2	1.62	1.77 ± 0.27**	0.875	0.418
	36:3	2.15	1.81 ± 0.31**	0.917	0.052
	36:4	1.95	1.93 ± 0.38**	0.958	0.901
	38:4	1.68	1.61 ± 0.22**	0.917	0.721
	38:5	1.84	2.26 ± 0.39**	0.958	0.142
	40:6	1.89	2.35 ± 0.39**	0.938	0.112
SM	d34:1	1.76	2.09 ± 0.24**	0.979	0.075
	d34:2	1.66	1.77 ± 0.22**	0.854	0.517
	d36:1	1.84	2.29 ± 0.32**	0.979	0.077
	d36:2	1.85	2.13 ± 0.39**	0.917	0.22
	d38:2	1.62	2.21 ± 0.38**	0.979	0.002
	d42:2	1.74	2.49 ± 0.34**	1.000	0.006

* $p < 0.05$;
** $p < 0.01$.

Table 2
Percent relative standard deviation (%RSD) value of the concentration of the five lipid species between nUHPLC-ESI-MS/MS and mFlFFF-ESI-MS based on five replicate measurements.

	% RSD (Relative Standard Deviation)	
	nUHPLC-ESI-MS/MS	mFlFFF-ESI-MS
PC 34:1	5.5	3.1
PC 38:4	4.7	3.9
PE 38:4	3.7	2.3
PI 38:4	1.5	4.4
SM d42:2	2.2	2.4
Av	3.5	3.2

compared to benign ones [46]. While the PC species differed between the studies, our results also highlight significantly increased levels of PI, especially PI 38:4 (or PI 18:0/20:4), which predominated among the PI species identified. PI plays a pivotal role in triggering the release of arachidonic acid (AA, 20:4), a precursor to eicosanoids such as prostaglandins and leukotrienes which are key mediators of inflammation and immune responses. This release is critical for activating inflammatory pathways that, in cancer, can exacerbate inflammation and promote tumor progression and metastasis [47,48]. Elevated levels of PI 38:4 in eCCA may thus promote chronic inflammation and oncogenic signaling pathways. Furthermore, the metabolic pathways of eicosanoids, including COX-2-derived prostaglandins, have been found to be upregulated in various cancers. These pathways are closely linked to PI metabolism, particularly through interactions with the PI3K-AKT signaling cascade, a major driver of tumorigenesis. Collectively, the upregulation of PI 38:4 highlights its pathological relevance in eCCA by fostering inflammation and activating cancer-associated molecular pathways [49,50].

4. Conclusion

This study demonstrates the optimization of a miniaturized flow field-flow fractionation (mFlFFF) technique combined with multi-angle light scattering (MALS) and ultraviolet (UV) detection for the efficient separation and characterization of exosomes derived from serum, particularly focusing on their lipid profiles in patients with extrahepatic cholangiocarcinoma (eCCA) by hyphenating mFlFFF with ESI-MS. The mFlFFF setup effectively resolved particles in the size range of ~20–200 nm in diameter, which includes the typical size of exosomes. By optimizing flow rates and channel thickness, the technique was able to separate nanoparticles by size, allowing for a detailed analysis of exosomal lipid content via electrospray ionization-mass spectrometry (ESI-MS).

The lipidomic analysis of serum-derived exosomes was performed by comparing the exosomal lipid profiles from eCCA patients and healthy controls using both quantitative bottom-up lipidomics through ultra-high-performance liquid chromatography (UHPLC)-ESI-MS/MS and top-down mFlFFF-ESI-MS analysis. This comprehensive lipidomic analysis identified 1119 lipid species from the eCCA group and 1051 from the control group. Among them, 64 lipid species showed significant changes, with most lipids, including LPC, PC, PE, and PI, being increased in the eCCA group.

The lipidomic data obtained from mFlFFF-ESI-MS were further supported by principal component analysis (PCA) and statistical comparisons, showing clear separation between the eCCA and control groups, with most lipids significantly upregulated in the eCCA group. Additionally, the receiver operating characteristic (ROC) curve analysis indicated that 35 lipid species could distinguish eCCA from healthy controls with high accuracy, making these lipids potential biomarkers for eCCA diagnosis. These results align with previous studies reporting lipidomic alterations in other types of cholangiocarcinoma and HCC, but highlight unique lipid alterations in eCCA serum exosomes, especially the increase in LPC, PC, and PI. Notably, PI 38:4 (PI 18:0/20:4) involved in the release of AA was predominant in the eCCA group. PI's role in releasing AA is crucial in inflammatory responses, as AA is a precursor to eicosanoids, which modulate immune responses and inflammation. The release of AA via PI signaling is essential for activating inflammatory pathways, which can exacerbate inflammation in cancer, thereby contributing to tumor progression and metastasis.

While this study contributes significantly to the understanding of lipid alterations in eCCA, particularly in serum exosomes, it also underscores the challenges in correlating these lipidomic changes with the pathological mechanisms of the disease. Future studies are necessary to explore the functional roles of these lipids and their potential as diagnostic or therapeutic targets in cholangiocarcinoma. While this study focuses on the top-down lipid analysis of exosome particles without a preliminary lipid extraction utilizing sophisticated mFlFFF-ESI-MS, it also lays the foundation for developing accurate biomarkers for cancer detection and monitoring, utilizing exosomal lipid profiles as a key feature. It is also anticipated that mFlFFF-ESI-MS, which identifies exosome lipidomic changes, could be applied not only to eCCA but also to other cancers.

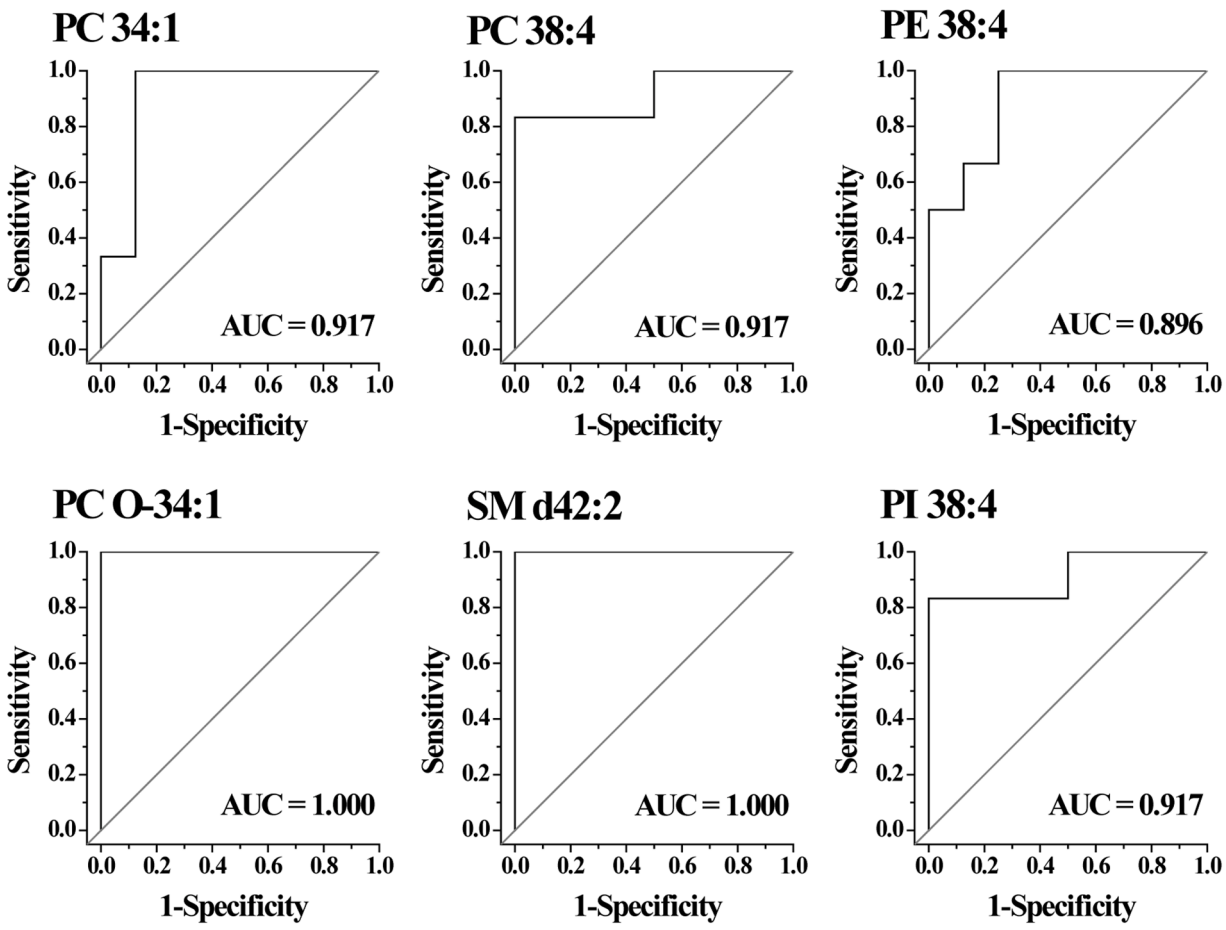

Fig. 6. Receiver operating characteristic (ROC) analysis of lipid biomarkers. Shown are representative ROC curves for six high-abundance lipid species with AUC > 0.800, indicating strong diagnostic potential for distinguishing eCCA from controls. The remaining ROC curves are provided in Figure S6.

CRediT authorship contribution statement

Hye Ju Yu: Writing – original draft, Formal analysis, Data curation, Conceptualization. **Myeong Hee Moon:** Writing – review & editing, Writing – original draft, Supervision, Project administration, Funding acquisition, Conceptualization.

Declaration of competing interest

The authors declare that they have no known competing financial interests or personal relationships that could have appeared to influence the work reported in this paper.

Acknowledgment

This work was supported by a grant (NRF-2021R1A2C2003171) supported by the National Research Foundation (NRF) of Korea.

Supplementary materials

Supplementary material associated with this article can be found, in the online version, at doi:10.1016/j.chroma.2025.465778.

Data availability

Data will be made available on request.

References

[1] K. Denzer, M.J. Kleijmeer, H.F. Heijnen, W. Stoorvogel, H.J. Geuze, Exosome: from internal vesicle of the multivesicular body to intercellular signaling device, J. Cell Sci. 113 (19) (2000) 3365–3374. Pt.
[2] C. Thery, L. Zitvogel, S. Amigorena, Exosomes: composition, biogenesis and function, Nat. Rev. Immunol. 2 (2002) 569–579.
[3] T. Skotland, N.P. Hessvik, K. Sandvig, A. Llorente, Exosomal lipid composition and the role of ether lipids and phosphoinositides in exosome biology, J. Lipid Res. 60 (2019) 9–18.
[4] E.R.J.T.C.R. Sauter, Exosomes in blood and cancer, 6 (2017) S1316–S1320.
[5] R.C. Lai, K.H. Tan, S.K. Lim, Membrane lipid binding molecules for the isolation of bona fide extracellular vesicle types and associated biomarkers in liquid biopsy, J. Cancer Metastasis Treat. 5 (2019) 65.
[6] E. Hosseini-Beheshti, S. Pham, H. Adomat, N. Li, E.S.T.J.M. Guns, c. proteomics, Exosomes as biomarker enriched microvesicles: characterization of exosomal proteins derived from a panel of prostate cell lines with distinct AR phenotypes, 11 (2012) 863–885.
[7] G. van Meer, D.R. Voelker, G.W. Feigenson, Membrane lipids: where they are and how they behave, Nat. Rev. Mol. Cell Biol. 9 (2008) 112–124.
[8] T. Skotland, K. Sandvig, A. Llorente, Lipids in exosomes: current knowledge and the way forward, Prog. Lipid Res. 66 (2017) 30–41.
[9] J. Donoso-Quezada, S. Ayala-Mar, J. González-Valdez, The role of lipids in exosome biology and intercellular communication: function, analytics and applications, Traffic 22 (2021) 204–220.
[10] C. Subra, K. Laulagnier, B. Perret, M. Record, Exosome lipidomics unravels lipid sorting at the level of multivesicular bodies, Biochimie 89 (2007) 205–212.
[11] C. Bruce, R.A. Chouinard, A.R. Tall, Plasma lipid transfer proteins, high-density lipoproteins, and reverse cholesterol transport, Annu. Rev. Nutr. 18 (1998) 297–330.
[12] K.R. Feingold, Introduction to Lipids and Lipoproteins, in: K.R. Feingold, B. Anawalt, M.R. Blackman, A. Boyce, G. Chrousos, E. Corpas, W.W. de Herder, K. Dhatariya, K. Dungan, J. Hofland, S. Kalra, G. Kaltsas, N. Kapoor, C. Koch, P. Kopp, M. Korbonits, C.S. Kovacs, W. Kuohung, B. Laferrere, M. Levy, E.A. McGee, R. McLachlan, M. New, J. Purnell, R. Sahay, A.S. Shah, F. Singer, M.A. Sperling, C.A. Stratakis, D.L. Trence, D.P. Wilson (Eds.) Endotext, South Dartmouth (MA), 2000.

[13] I. Rajman, M.J. Kendall, R. Cramb, R.L. Holder, M. Salih, M.D. Gammage, Investigation of low density lipoprotein subfractions as a coronary risk factor in normotriglyceridaemic men, Atherosclerosis 125 (1996) 231–242.
[14] S.K. Byeon, J.Y. Lee, S. Lim, D. Choi, M.H. Moon, Discovery of candidate phospholipid biomarkers in human lipoproteins with coronary artery disease by flow field-flow fractionation and nanoflow liquid chromatography-tandem mass spectrometry, J. Chromatogr. A 1270 (2012) 246–253.
[15] Z.H. Alshehry, P.A. Mundra, C.K. Barlow, N.A. Mellett, G. Wong, M.J. McConville, J. Simes, A.M. Tonkin, D.R. Sullivan, E.H. Barnes, P.J. Nestel, B.A. Kingwell, M. Marre, B. Neal, N.R. Poulter, A. Rodgers, B. Williams, S. Zoungas, G.S. Hillis, J. Chalmers, M. Woodward, P.J. Meikle, Plasma lipidomic profiles improve on traditional risk factors for the prediction of cardiovascular events in type 2 diabetes mellitus, Circulation 134 (2016) 1637. -+.
[16] B. Lidgard, A.N. Hoofnagle, L.R. Zelnick, I.H. de Boer, A.M. Fretts, B. R. Kestenbaum, R.N. Lemaitre, C. Robinson-Cohen, N. Bansal, High-density lipoprotein lipidomics in chronic kidney disease, Clin. Chem. 69 (2023) 273–282.
[17] J.Y. Kim, G.B. Lee, J.C. Lee, M.H. Moon, High-speed screening of lipoprotein components using online miniaturized asymmetrical flow field-flow fractionation and electrospray ionization tandem mass spectrometry: application to hepatocellular carcinoma plasma samples, Anal. Chem. 93 (2021) 4867–4875.
[18] G. Andreotti, J.B. Chen, Y.T. Gao, A. Rashid, S.C. Chang, M.C. Shen, B.S. Wang, T. Q. Han, B.H. Zhang, K.N. Danforth, M.D. Althuis, A.W. Hsing, Serum lipid levels and the risk of biliary tract cancers and biliary stones: a population-based study in China, Int. J. Cancer 122 (2008) 2322–2329.
[19] J.H. Jung, K. Taniguchi, H.M. Lee, M.Y. Lee, R. Bandu, K. Komura, K.Y. Lee, Y. Akao, K.P. Kim, Comparative lipidomics of 5-fluorouracil-sensitive and -resistant colorectal cancer cells reveals altered sphingomyelin and ceramide controlled by acid sphingomyelinase (SMPD1), Sci. Rep. 10 (2020) 6124.
[20] J.H. Yoon, Y. Seo, Y.S. Jo, S. Lee, E. Cho, A. Cazenave-Gassiot, Y.S. Shin, M. H. Moon, H.J. An, M.R. Wenk, P.G. Suh, Brain lipidomics: from functional landscape to clinical significance, Sci. Adv. 8 (2022) eadc9317.
[21] J. Xu, A.M. Casas-Ferreira, Y. Ma, A. Sen, M. Kim, P. Proitsi, M. Shkodra, M. Tena, P. Srinivasan, N. Heaton, W. Jassem, C. Legido-Quigley, Lipidomics comparing DCD and DBD liver allografts uncovers lysophospholipids elevated in recipients undergoing early allograft dysfunction, Sci. Rep. 5 (2015) 17737.
[22] G.B. Lee, J.C. Lee, M.H. Moon, Plasma lipid profile comparison of five different cancers by nanoflow ultrahigh performance liquid chromatography-tandem mass spectrometry, Anal. Chim. Acta 1063 (2019) 117–126.
[23] J.Y. Eum, J.C. Lee, S.S. Yi, I.Y. Kim, J.K. Seong, M.H. Moon, Aging-related lipidomic changes in mouse serum, kidney, and heart by nanoflow ultrahigh-performance liquid chromatography-tandem mass spectrometry, J. Chromatogr. A 1618 (2020) 460849.
[24] J. Graessler, C.S. Mehnert, K.M. Schulte, S. Bergmann, S. Strauss, T.D. Bornstein, J. Licinio, M.L. Wong, A.L. Birkenfeld, S.R. Bornstein, Urinary lipidomics: evidence for multiple sources and sexual dimorphism in healthy individuals, Pharmacogenomics J. 18 (2018) 331–339.
[25] M. Caterino, R. Fedele, V. Carnovale, A. Castaldo, M. Gelzo, P. Iacotucci, M. Ruoppolo, G. Castaldo, Lipidomic alterations in human saliva from cystic fibrosis patients, Sci. Rep. 13 (2023) 600.
[26] G.B. Lee, A. Caner, M.H. Moon, Optimisation of saliva volumes for lipidomic analysis by nanoflow ultrahigh performance liquid chromatography-tandem mass spectrometry, Anal. Chim. Acta 1193 (2022) 339318.
[27] J.C. Giddings, Field-flow fractionation: analysis of macromolecular, colloidal, and particulate materials, Science 260 (1993) 1456–1465.
[28] M.H. Moon, Flow field-flow fractionation: recent applications for lipidomic and proteomic analysis, Trac-Trend Anal. Chem. 118 (2019) 19–28.
[29] K.G. Wahlund, H.S. Winegarner, K.D. Caldwell, J.C. Giddings, Improved flow field-flow fractionation system applied to water-soluble polymers: programming, outlet stream splitting, and flow optimization, Anal. Chem. 58 (1986) 573–578.
[30] P. Reschiglian, A. Zattoni, B. Roda, S. Casolari, M.H. Moon, J. Lee, J. Jung, K. Rodmalm, G. Cenacchi, Bacteria sorting by field-flow fractionation. Application to whole-cell Escherichia coil vaccine strains, Anal. Chem. 74 (2002) 4895–4904.
[31] S. Sitar, A. Kejzar, D. Pahovnik, K. Kogej, M. Tusek-Znidaric, M. Lenassi, E. Zagar, Size characterization and quantification of exosomes by asymmetrical-flow field-flow fractionation, Anal. Chem. 87 (2015) 9225–9233.
[32] Y.B. Kim, J.S. Yang, G.B. Lee, M.H. Moon, Evaluation of exosome separation from human serum by frit-inlet asymmetrical flow field-flow fractionation and multiangle light scattering, Anal. Chim. Acta 1124 (2020) 137–145.
[33] K.E. Petersen, E. Manangon, J.L. Hood, S.A. Wickline, D.P. Fernandez, W. P. Johnson, B.K. Gale, A review of exosome separation techniques and characterization of B16-F10 mouse melanoma exosomes with AF4-UV-MALS-DLS-TEM, Anal. Bioanal. Chem. 406 (2014) 7855–7866.
[34] J.S. Yang, J.C. Lee, S.K. Byeon, K.H. Rha, M.H. Moon, Size dependent lipidomic analysis of urinary exosomes from patients with prostate cancer by flow field-flow fractionation and nanoflow liquid chromatography-tandem mass spectrometry, Anal. Chem. 89 (2017) 2488–2496.
[35] Y.H. Shaib, J.A. Davila, K. McGlynn, H.B. El-Serag, Rising incidence of intrahepatic cholangiocarcinoma in the United States: a true increase? J. Hepatol. 40 (2004) 472–477.
[36] O. Clements, J. Eliahoo, J.U. Kim, S.D. Taylor-Robinson, S.A. Khan, Risk factors for intrahepatic and extrahepatic cholangiocarcinoma: a systematic review and meta-analysis, J. Hepatol. 72 (2020) 95–103.
[37] R. Montal, D. Sia, C. Montironi, W.Q. Leow, R. Esteban-Fabró, R. Pinyol, M. Torres-Martin, L. Bassaganyas, A. Moeini, J. Peix, Molecular classification and therapeutic targets in extrahepatic cholangiocarcinoma, J. Hepatol. 73 (2020) 315–327.
[38] P. Bertuccio, M. Malvezzi, G. Carioli, D. Hashim, P. Boffetta, H.B. El-Serag, C. La Vecchia, E. Negri, Global trends in mortality from intrahepatic and extrahepatic cholangiocarcinoma, J. Hepatol. 71 (2019) 104–114.
[39] L.P. Mocan, M. Ilies, C.S. Melincovici, M. Sparchez, R. Craciun, I. Nenu, A. Horhat, C. Tefas, Z. Sparchez, C.A. Iuga, T. Mocan, C.M. Mihu, Novel approaches in search for biomarkers of cholangiocarcinoma, World J. Gastroenterol. 28 (2022) 1508–1525.
[40] S.A. Lang, J. Bednarsch, K. Joechle, I. Amygdalos, Z. Czigany, L. Heij, T.F. Ulmer, U.P. Neumann, Prognostic biomarkers for cholangiocarcinoma (CCA): state of the art, Expert Rev. Gastroent. 15 (2021) 497–510.
[41] M.H. Zhang, S.S. Cheng, Y. Jin, Y.Q. Zhao, Y. Wang, Roles of CA125 in diagnosis, prediction, and oncogenesis of ovarian cancer, BBA-Rev. Cancer (2021) 1875.
[42] Y.S. Park, C.W. Yoo, S.C. Lee, S.J. Park, J.H. Oh, B.C. Yoo, S.S. Paik, K.G. Lee, S. Y. Jin, S.C. Kim, K.P. Kim, Y.H. Kim, D. Choi, H.K. Kim, Lipid profiles for intrahepatic cholangiocarcinoma identified using matrix-assisted laser desorption/ionization mass spectrometry, Clinica Chimica Acta 412 (2011) 1978–1982.
[43] T. Zhao, H.J. Zhang, X.L. Zhang, T.T. Zhao, H.Y. Lan, Q.L. Liang, G.A. Luo, P. Li, Metabolomic and lipidomic study of the protective effect of Chaihuang-Yishen formula on rats with diabetic nephropathy, J. Ethnopharmacol. 166 (2015) 31–41.
[44] J.P. Koelmel, N.M. Kroeger, C.Z. Ulmer, J.A. Bowden, R.E. Patterson, J.A. Cochran, C.W. Beecher, T.J. Garrett, R.A. Yost, LipidMatch: an automated workflow for rule-based lipid identification using untargeted high-resolution tandem mass spectrometry data, BMC Bioinformatics 18 (2017) 1–11.
[45] Q. Liang, C. Wang, B.B. Li, A.H. Zhang, Lipidomics analysis based on liquid chromatography mass spectrometry for hepatocellular carcinoma and intrahepatic cholangiocarcinoma, in: RSC Adv, 5, 2015, pp. 63711–63718.
[46] R. Muraki, Y. Morita, S. Ida, R. Kitajima, S. Furuhashi, M. Takeda, H. Kikuchi, Y. Hiramatsu, Y. Takanashi, Y. Hamaya, K. Sugimoto, J. Ito, K. Kawata, H. Kawasaki, T. Sato, T. Kahyo, M. Setou, H. Takeuchi, Phosphatidylcholine in bile-derived small extracellular vesicles as a novel biomarker of cholangiocarcinoma, Cancer Med. 12 (2023) 13007–13018.
[47] H. Makinoshima, S. Umemura, A. Suzuki, H. Nakanishi, A. Maruyama, H. Udagawa, S. Mimaki, S. Matsumoto, S. Niho, G. Ishii, M. Tsuboi, A. Ochiai, H. Esumi, T. Sasaki, K. Goto, K. Tsuchihara, Metabolic determinants of sensitivity to phosphatidylinositol 3-kinase pathway inhibitor in small-cell lung carcinoma, Cancer Res. 78 (2018) 2179–2190.
[48] L. Gozzelino, M.C. De Santis, F. Gulluni, E. Hirsch, M. Martini, PI (3,4)P2 signaling in cancer and metabolism, Front. Oncol. (2020) 10.
[49] M. Hughes-Fulford, C.F. Li, L. Boonyaratanakornkit, S. Sayyah, Arachidonic acid activates phosphatidylinositol 3-kinase signaling and induces gene expression in prostate cancer, Cancer Res. 66 (2006) 1427–1433.
[50] A.M. Johnson, E.K. Kleczko, R.A. Nemenoff, Eicosanoids in cancer: new roles in immunoregulation, Front. Pharmacol. 11 (2020).